EasyChair Preprint

№ 2748

First-principles Calculations of Optoelectronic Properties of Sn1-xInxA (A= S and Se) for Solar Cell Applications

Zeesham Abbas, Sabeen Munaf, Sikander Azam, Muhammad Abubakar and Muhammad Irfan

February 22, 2020

First-principles Calculations of Optoelectronic Properties of $Sn_{1-x}In_x$ A (A= S and Se) for Solar Cell Applications

Zeesham Abbas[1], Sabeen Munaf[1], Sikander Azam[2], Muhammad Abubakr[1], Muhammad Irfan[1]

[1]Department of Physics, The University of Lahore, Sargodha campus, 40100 Sargodha, Pakistan

[2]Faculty of Engineering and Applied Sciences, Department of Physics, RIPHAH International University I-14 Campus, Islamabad, Pakistan

* Correspondence:

ABSTRACT

Influence the transition metals atom(s) on the optoelectronic features of the $Sn_{1-x}In_xA$ (A= S and Se) is explored theoretically. The electronic and optoelectronic features are explored within the DFT based FP-LAPW method. Additionally, PBE-GGA is applied for computing of their structural properties. The electronic and optical features are calculated using GGA. We have discovered that both the compounds are metallic. We explore in details atomic/orbital origin of electronic states in the band structure for the Se/S and Sn containing materials from the spectra of electronic density of states. The optical properties are evaluated following the spectra of optical function along with the other related optical properties like energy loss function, reflectivity, refractive index, extinction coefficient, and conductivity dispersion. The study of optical properties of the In based material confirms that these materials can be promising for the design of optoelectronic devices with the desired properties.

INTRODUCTION

Materials with intermediate band attracted the attention of scientists for applications in solar cells over last few decades [1]. The concept of intermediate band was proposed by developing the IB photovoltaic materials in order to overcome the problem of efficiency in the next generation solar cells. The working model of these solar cells is shown in Fig. 1.

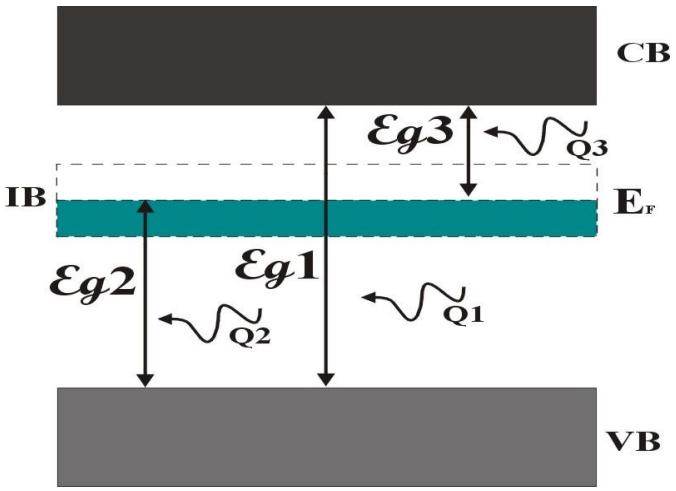

Fig. 1: Model of intermediate band solar cell

Possible transitions of electrons are specified by the arrows. This Transitions of electrons by traditional process also takes place from VB to CB. In the above figure, $\mathcal{E}_{g1}$, $\mathcal{E}_{g2}$ and $\mathcal{E}_{g3}$ are the energy gaps between VB-CB, VB-IB and IB-CB, respectively, and Fermi energy is shown by E_F. It can also be noted that electrons with lower energy than $\mathcal{E}_{g1}$ can stay in this intermediate band while traveling from VB to CB. While utilizing the partially filled MIB, electrons can travel to IB from VB and then to CB from IB.

Several characteristics of MIB based solar cells are shown in Fig. 1. Presence of an isolated IB between VB and CB can be focused among these characteristics. If this condition is not satisfied, thermal relaxations can be produced as a result of the interaction among the phonons coming from the crystal lattice and the electrons. Furthermore, the IB should have a specified thickness in order to avoid the phenomenon of non-radiative recombination as much as possible. The IB should be partially empty so that it must be able to accommodate the electrons coming from VB to IB by absorbing the photons with lower energies and then travel to CB from this one.

Solar cells with this structure shows higher efficiencies as compared to those established by the Shockley limit [2], as revealed in the earlier study of Luque and Marti [1]. They show the increase in efficiency through the operation of these solar cells and the thermodynamic arguments. Materials with intermediate band can be prepared by introducing quantum dots in the geometry [3] or by using II-VI diluted oxides [4].

To study the electronic and optical properties of $Sn_{1-x}In_xA$ (A= S and Se) having intermediate band by using quantum mechanical methodology is the main focus of this study. Furthermore, this methodology will also be used for calculations of electronic and optical properties of the aforementioned compound. First of all, we will present the methodology (approximation) that we will use to calculate electronic properties and then optical properties.

METHODOLOGY

Full potential linearized augmented plane wave (FP-LAPW) [5] method was used to solve Kohn-Sham equations in order to calculate physical properties of the compounds under study using self-consistent approach within the frame work of DFT [6, 7] (density functional theory) as implemented in WIEN2k code [8, 9]. GGA (generalized gradient approximation) approach was used to treat E_{xc} (exchange correlation energy) while calculating electronic and optical properties of $Sn_{1-x}In_xA$ (A= S and Se). Theoretical studies of aforementioned compound were carried out by using optimized geometry achieved by minimizing forces on the atoms of the unit cell.

There are two regions in the unit cell of the crystal while using FP-LAPW method i.e. interstitial region (IR) and muffin-tin (atomic spheres). Here, valance and core electrons are the two groups of electron that are treated separately. Muffin-tin (MT) model is used to specify crystal potential in this technique. Interstitial region is formed by valance electrons whereas non-overlapping atomic spheres having radius R_{MT} (smallest muffin-tin radius). Spherical harmonics (Y_{lm}) times the radial solution of Schrodinger wave equation (SWE) for single particle at fixed energy (V_{lm}).

$$V(r) = \sum_{l,m} V_{lm}(r) Y_{lm}(r) \tag{1}$$

On the other hand, basis of plane wave is used to expand wave function in IR of the unit cell by using following relation:

$$V(r) = \sum_{k} V_k e^{i\vec{k}.\vec{r}} \tag{2}$$

The calculations were performed by taking 500 k-points and $R_{MT}k_{max} = 7$ (R_{MT} and k_{max} are smallest value of muffin-tin radius and cut-of wave vector of the plane wave basis, respectively). Value of maximum angular momentum was taken as l_{max} =10. Step size of the charge density is set as $0.00001 e a_0^{-3}$ to terminate iterations and is known as convergence criterion.

Separation between core and valance states (core cut-off energy) is taken as -8Ry. Unit cell of $Sn_{1-x}In_xSe$ is shown in Fig. 1.

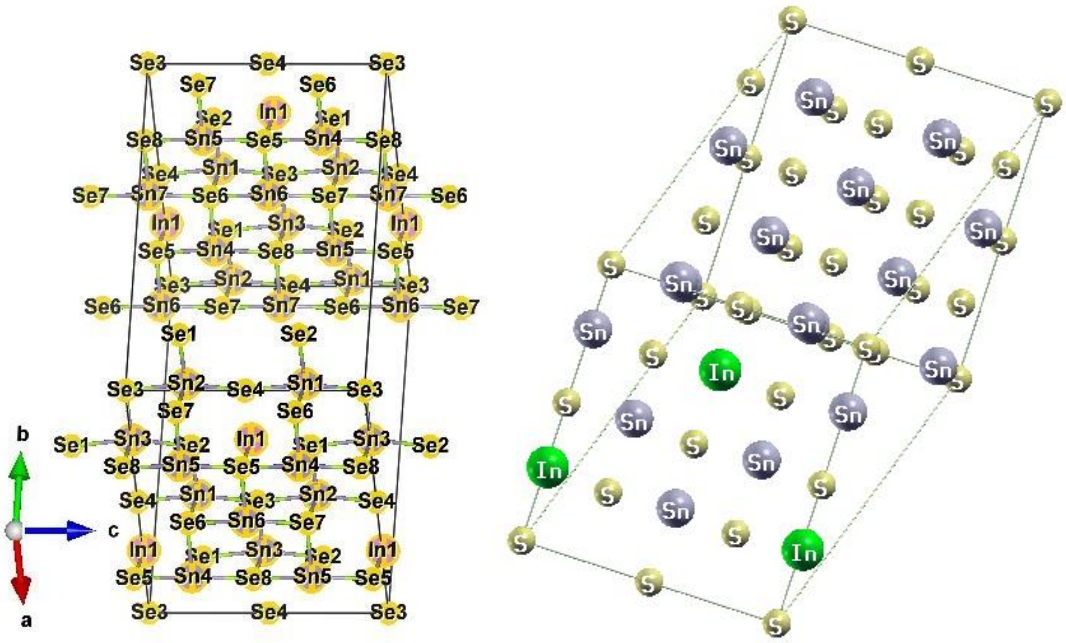

Fig. 1: Unit cell of $Sn_{1-x}In_xSe$ and $Sn_{1-x}In_xS$

RESULTS AND DISCUSSION

ELECTRONIC PROPERTIES

We calculated the electronic properties of $Sn_{1-x}In_xA$ (A= S and Se) in this section; namely the band structure, the band gap and the density of states. Density of states are plotted a continuous energy range (-5 to 6 eV) to determine different electronic contributions in conduction and valance bands. Electronic band structure is also plotted for continuous energy range (-5 to 5 eV) along high symmetric points of Brillouin zone.

BAND STRUCTURE

Band structure of the supercell of $Sn_{1-x}In_xA$ (A= S and Se) is discussed in this section. Calculated electronic band structure for $Sn_{1-x}In_xA$ (A= S and Se) along high symmetry points of the Brillouin zone is shown in Fig. 2. In the plotted band structure, Fermi energy level is set at 0.0 eV. An extra band known as intermediate band can be seen in the band gap. Completely isolated intermediate band (IB) in the band structure of $Sn_{1-x}In_xA$ (A= S and Se)is shown in Fig. 2 with blue box. We can see that Fermi energy level cross this intermediate band. There are three different types of intermediate bands depending on the number of electrons in the IB: (i) type I (completely

empty), (ii) type II (partially filled) and (iii) type III (completely empty), as shown in Fig. 3. Type III and I of the IB can be used as charge storage as they can store electronic charge in the form of electrons or holes, respectively [10]. Numerous materials have been reported that possess intermediate band for applications in Li-ion batteries like $LiMn_2O_4$, $LiCoO_2$ etc [11]. Due to partially filled IB, $Sn_{1-x}In_xA$ (A= S and Se) is an appropriate material for solar cells with intermediate band. In this article, main focus is on the compound having type II intermediate band.

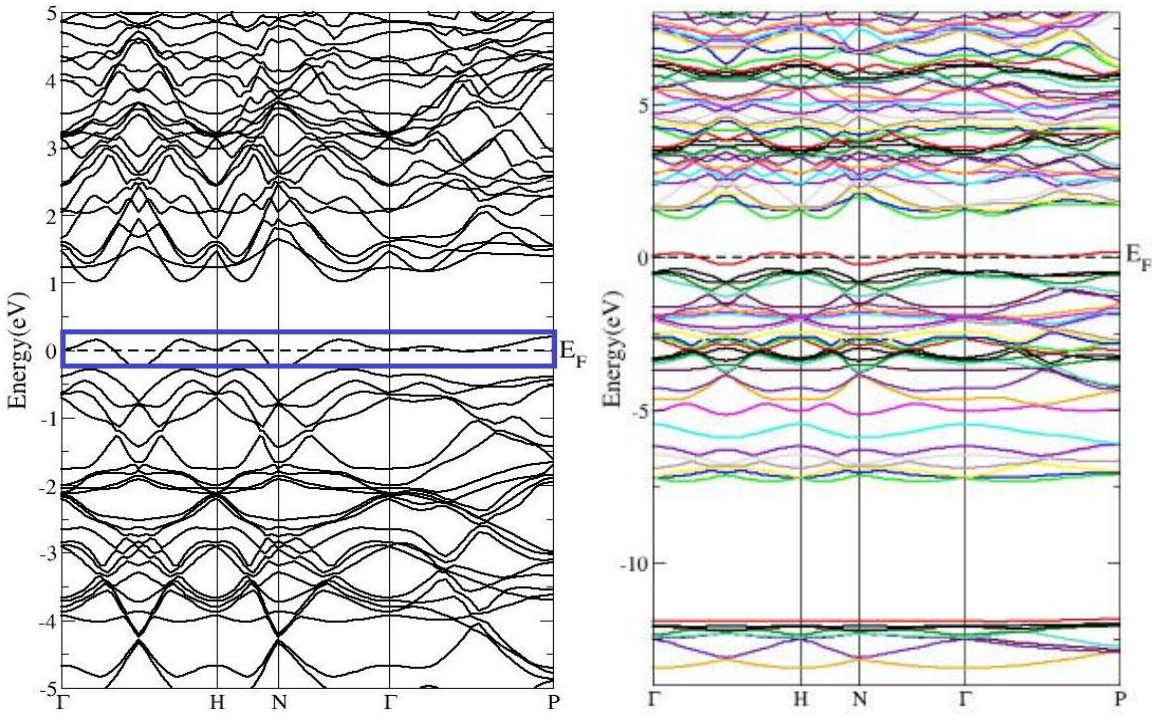

Fig. 2: Electronic band structure of (a) $Sn_{1-x}In_xSe$ and (b) $Sn_{1-x}In_xS$

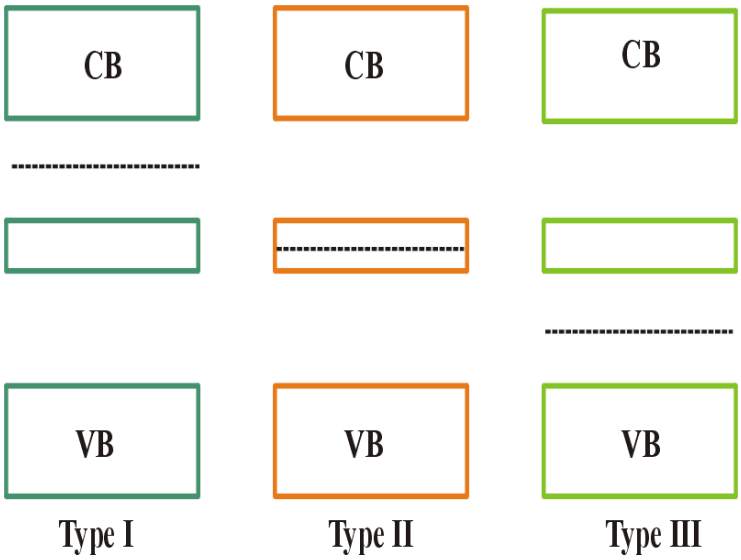

Fig. 2: Types of intermediate band w.r.t. position of Fermi level

DENSITY OF STATES

Total density of states (TDOS) and partial density of states (PDOS) are also calculated in order to describe contributions of different orbitals in the material. Plotted TDOS and PDOS are shown in Fig. 3. It can be noticed that major contributions in valance band come from Se atoms and some minor contributions from Sn atoms. However, an intermediate band of In and Se atoms is present around Fermi level (-0.25 to 0.25 eV). In conduction band, major contributions come from Sn and Se atoms. However, In atoms also have minor contributions in conduction band.

From the plots of PDOS, it can be noted that valance band can be divided into three section i.e. first section (-5 to -4 eV), second section (-4 to -2 eV) and third section (-2 to 0.25 eV). In first section, major contributions come from In(s), Sn(p) and Se/S(p) orbitals. Second section of valance band mainly consists of Sn(p) and Se(p) orbitals, however, some minor contributions from In(p) orbitals. And major contributions in third section of valance band come from Se/S(p), Sn(p), Sn(p), however, strong contributions of In(s) and In(p) are present around Fermi level (above and below 0 eV). From the plots of PDOS, it can be noted that major contributions in conduction band come from In(p), Sn(p) and Se/S(p) orbitals, however, Sn (s) and In(s) orbitals also have some minor contributions in conduction band of $Sn_{1-x}In_xSe$.

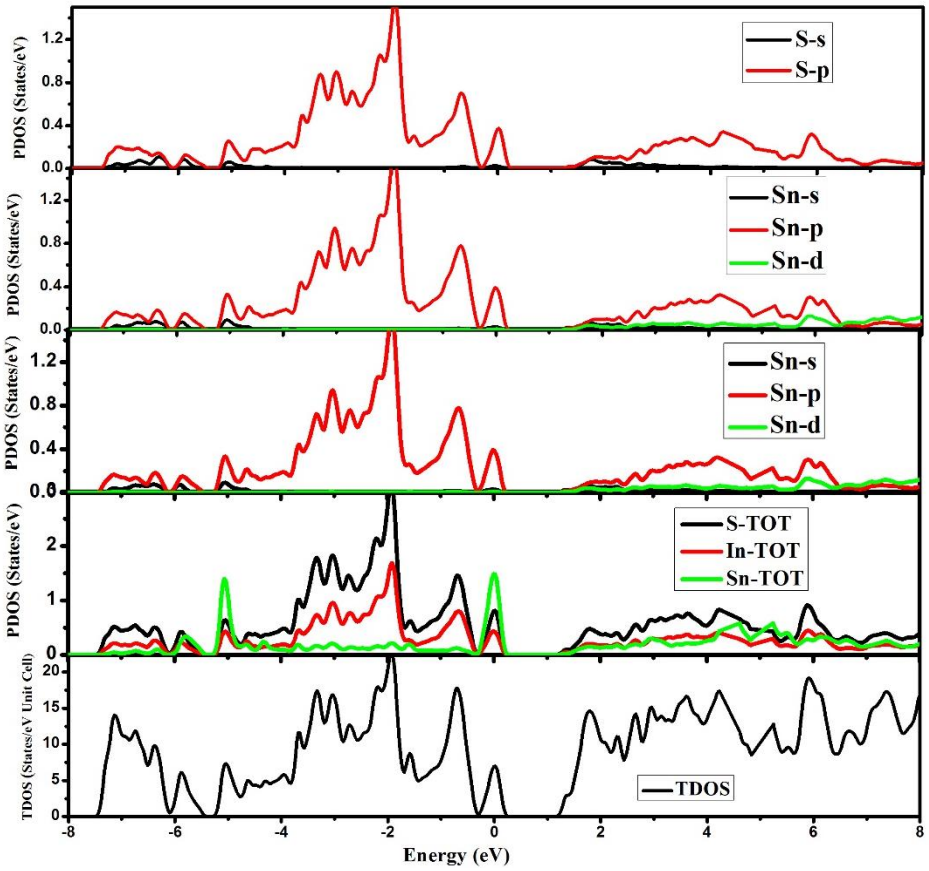
PDOS (States/eV)
S-s
S-p
Sn-s
Sn-p
Sn-d
Sn-s
Sn-p
Sn-d
S-TOT
In-TOT
Sn-TOT
TDOS (States/eV Unit Cell)
TDOS
Energy (eV)

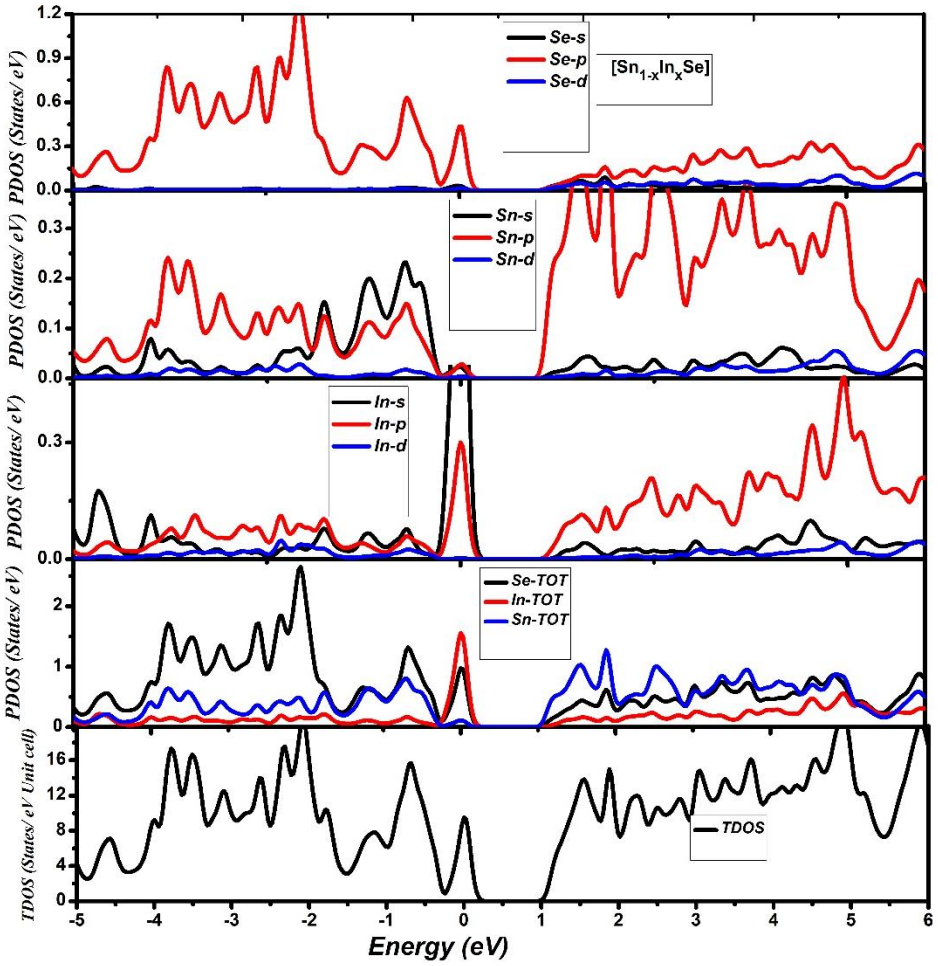

Fig. 3: Total and partial density of states for $Sn_{1-x}In_xSe$

Fermi Surface

Fermi surface (FS) is calculated for the reachable electronic orbital of $Sn_{1-x}In_xSe$ due to its metallic nature. Near Fermi band configuration of $Sn_{1-x}In_xSe$ along the high-symmetry lines selected in first Brillion zone of the tetragonal crystal is shown in Fig. 4 along high symmetry points of the first Brillouin zone. Vital role in conductivity is played by the electrons present near the Fermi level. Fermi Surface (FS) of the any metallic material can be used to understand its electronic structure (density of states and band structure). Fermi surface is calculated in order to get comprehensive information of the electronic states at the Fermi level. Fermi surface of $Sn_{1-x}In_xSe$ is shown in this article to get better description of the electronic states crossing the E_F. We have shown There are two regions in the plot of FS i.e. colored region and empty spaces which shows electronic sheets and holes, respectively. There is only one band crossing the Fermi level

(E_F) in the investigated compound. Different electrons in the system are defined by Fermi surface whose topography is directly related to the thermoelectric properties of the materials like electrical conductivity. Layers with different colors shows electrons with different velocities. Electrons in red layers have higher velocities as compared to the electrons in blue layers.

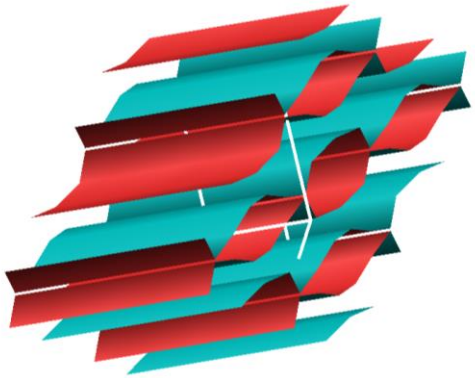

Fig. 4: Fermi surface for $Sn_{1-x}In_xSe$

Optical Properties

In this section, we investigated optical properties of $Sn_{1-x}In_xA$ (A= S and Se) in order to explore potential applications of aforementioned compound in telecommunication, solar cell and optoelectronic technologies. Following relations are used to calculate optical conductivity $\sigma(\omega)$, extinction coefficient $k(\omega)$, refractive index $n(\omega)$, energy loss function $L(\omega)$, absorption coefficient $I(\omega)$ and dielectric function $\varepsilon(\omega)$ [12, 13].

$$\varepsilon_{1(\omega)} = 1 + \frac{2}{\pi} P \int_0^{\infty} \frac{\omega' \varepsilon_2(\omega')}{\omega'^2 - \omega^2} d\omega' \tag{3}$$

$$\varepsilon_2(\omega) = \frac{e^2 h'}{\pi m^2 \omega^2} \sum_{v,c} \int_{BZ}^{\infty} |M_{cv}(k)|^2 \delta[\omega_{cv}(k) - \omega] d^3k \tag{4}$$

$$n(\omega) = \left[\frac{\varepsilon_1(\omega)}{2} + \frac{\sqrt{\varepsilon_1^2(\omega) + \varepsilon_2^2(\omega)}}{2} \right]^{1/2} \tag{5}$$

$$k(\omega) = \left[-\frac{\varepsilon_1(\omega)}{2} + \frac{\sqrt{\varepsilon_1^2(\omega) + \varepsilon_2^2(\omega)}}{2} \right]^{1/2} \tag{6}$$

$$R(\omega) = \frac{(n-1)^2 + k^2}{(n+1)^2 + k^2} \tag{7}$$

$$\alpha(\omega) = 4\pi k(\omega)/\lambda \quad (8)$$

$$\sigma(\omega) = (2W_{cv}h'\omega)/E_0 \quad (9)$$

$$L(\omega) = Im(-1/\tilde{\varepsilon}(\omega)) \quad (8)$$

Where transition rate per unit time is specified by W_{cv}.

Complex dielectric function can be used to discuss the type of interaction between $Sn_{1-x}In_xSe$ and the incoming photons. Following relation can be used to calculate complex dielectric function:

$$\varepsilon(\omega) = \varepsilon_1(\omega) + i\varepsilon_2(\omega) \quad (9)$$

Where $\varepsilon_1(\omega)$ is known as real part of dielectric function and it describes the dispersion of light as a result of interaction between photons and host lattice. And $\varepsilon_2(\omega)$ is known as imaginary part of complex dielectric function and it can be used to explain the absorption of photons as a result of electronic transitions between different bands of the material. Kramer-Kronig relation can be used to relate these parameters [14, 15] and these parameters are used to calculate all other optical parameters over photon energy range of 0-14 eV.

Real part $\varepsilon_1(\omega)$ and imaginary part $\varepsilon_2(\omega)$ of complex dielectric function is shown in Fig. 5 (a) and (b), respectively. Chalcogenide compound ($Sn_{1-x}In_xA$ (A= S and Se)) belongs to tetragonal crystal system and the three main components of complex dielectric function are $\varepsilon^{xx}(\omega) = \varepsilon^{yy}(\omega)$ and $\varepsilon^{xx}(\omega)$. Highest peaks in the spectra of $\varepsilon_1^{xx}(\omega)$ and $\varepsilon_1^{zz}(\omega)$ are present in infrared and visible region. After 2.0 eV, both curves of $\varepsilon_1^{xx}(\omega)$ and $\varepsilon_1^{zz}(\omega)$ decrease continuously and becomes negative at approximately 5.7 and 2.6 eV, respectively. These negative values of both components of real part $\varepsilon_1(\omega)$ shows metal like reflecting nature of $Sn_{1-x}In_xSe$. Computed spectra can also be used to determine an important quantity known as static values of real part $\varepsilon_1(0)$ of complex dielectric function. Values of static dielectric constant for $\varepsilon_1^{xx}(0)$ and $\varepsilon_1^{zz}(0)$ of $Sn_{1-x}In_xSe$ are approximately 9.8 and 19.9, respectively. Penn's model can be used to explain this property by the following relation [16] and one can conclude that materials having larger value of E_g have lower values of $\varepsilon_1(0)$:

$$\varepsilon_1(0) \approx 1 + \left(\frac{\hbar\omega p}{E_g}\right)^2 \quad (10)$$

Imaginary part $\varepsilon_2(\omega)$ of complex dielectric is used to explain absorption of incoming photons by the interacting material. A unique parameter in the spectra of $\varepsilon_2(\omega)$ is its critical value that is directly related to threshold energy above and below which $Sn_{1-x}In_xA$ (A= S and Se) shows absorption and transmission of photons, respectively. One can notice that critical value in the spectra of compound under study lie below 0 eV which shows that all the photons are absorbed by this material and no transmission is present. Highest peaks in the spectra of $\varepsilon_2^{xx}(\omega)$ and $\varepsilon_2^{zz}(\omega)$ are present at approximately 2.4 and 2.0 eV, respectively. After that both curves start reducing and other smaller peaks are present around 5.4 and 6.7 eV in the spectra of $\varepsilon_1^{xx}(\omega)$ and $\varepsilon_1^{zz}(\omega)$, respectively. After these minor peaks due to different electronic transitions, $\varepsilon_2(\omega)$ becomes zero at 13.5 eV.

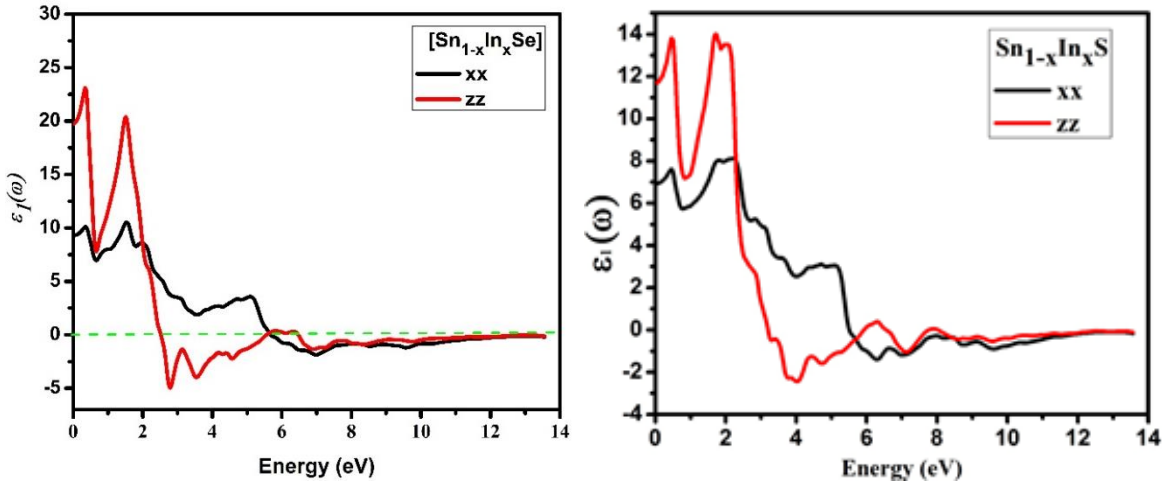

(a) (b)

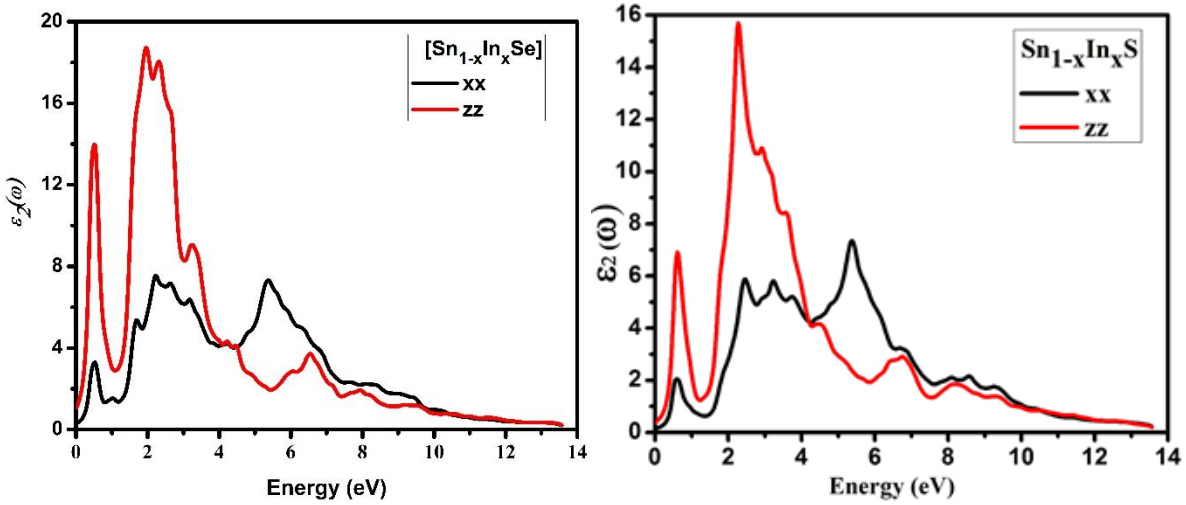

(c) (d)

Fig. 5: (a) Real part $\varepsilon_1(\omega)$ and (b) imaginary part $\varepsilon_2(\omega)$ of complex dielectric function for $Sn_{1-x}In_xSe$

Calculated spectra of refractive index $n(\omega)$ and extinction coefficient $k(\omega)$ for $Sn_{1-x}In_xA$ (A= S and Se) are shown in Fig. 6 (a) and (b). Following relations can also be used to calculate extinction coefficient ($k(\omega)$) and refractive index ($n(\omega)$) from the calculated values of real part $\varepsilon_1(\omega)$ and imaginary part $\varepsilon_2(\omega)$ of complex dielectric function:

$$\varepsilon_1(\omega) = n^2 - k^2 \tag{11}$$

$$\varepsilon_2(\omega) = 2nk \tag{12}$$

Dispersion and transparency characteristics of the material can be explained by refractive index $n(\omega)$. Highest peaks in the spectra of $n^{xx}(\omega)$ and $n^{zz}(\omega)$ are present in infrared and visible region at approximately 1.7 and 0.5 eV, respectively. After 2.5 eV, both curves of $n^{xx}(\omega)$ and $n^{zz}(\omega)$ decrease continuously and becomes less than one at approximately 7.1 and 6.9 eV, respectively, which shows that group velocity $\left(V_g = c/n\right)$ becomes greater than speed of light [17] and polarization of $Sn_{1-x}In_xA$ (A= S and Se) opposes these energies of photons. Computed spectra of refractive index $n(\omega)$ can also be used to determine an important quantity known as static refractive index $n(0)$. Values of static refractive index for $n^{xx}(0)$ and $n^{zz}(0)$ of $Sn_{1-x}In_xA$ (A= S and Se) are approximately 3.05 and 4.45, respectively. following relation is satisfied by the static values of real part $\varepsilon_1(0)$ and refractive index $n(0)$:

$$n(0) = \sqrt{\varepsilon_1(0)} \tag{13}$$

Absorption of energy and other similar features to that of imaginary part $\varepsilon_2(\omega)$ of complex dielectric function are explained by extinction coefficient $k(\omega)$. Like $\varepsilon_2(\omega)$, extinction coefficient $k(\omega)$ also have some minor values at 0 eV which shows that all the incident photons are absorbed by the target material. Highest peaks ($k_{max}(\omega)$) in the spectra of extinction coefficient $k^{xx}(\omega)$ and $k^{zz}(\omega)$ occurs at approximately 5.6 and 2.7 eV, respectively. There are sharp peaks in infrared and visible region in the spectra of $k^{zz}(\omega)$. There is a sharp decrease in spectra of $k^{xx}(\omega)$ and $k^{zz}(\omega)$ after their peak values.

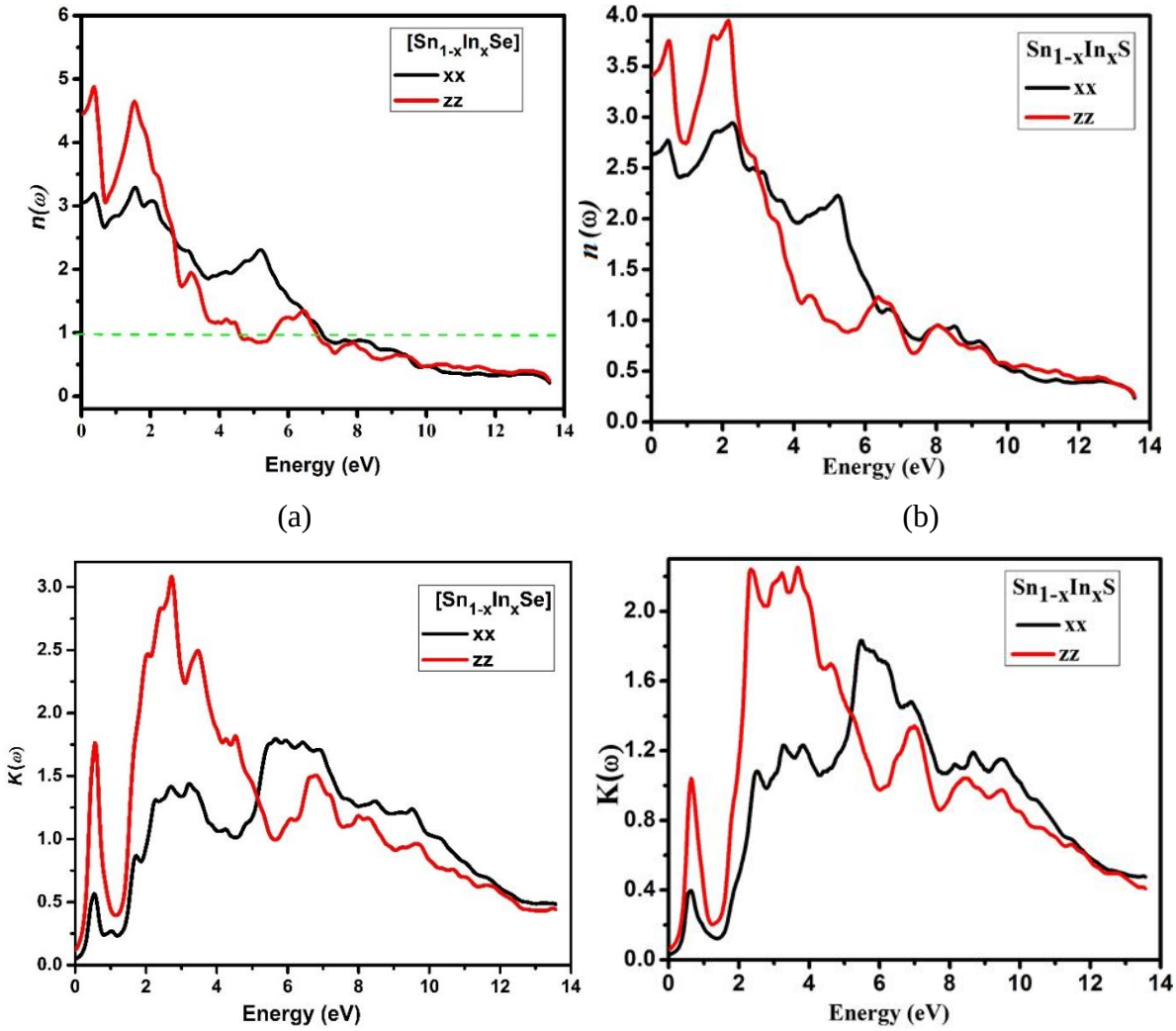

Fig. 6: (a) Refractive index $n(\omega)$ and (b) extinction coefficient $k(\omega)$ for $Sn_{1-x}In_xSe$

Calculated spectra of absorption coefficient $I(\omega)$ and reflectivity $R(\omega)$ for $Sn_{1-x}In_xSe$ are shown in Fig. 7 (a) and (b). The following relation can also be used to calculate absorption coefficient [18]:

$$\alpha(\omega) = \sqrt{2}\omega\left[\sqrt{\varepsilon_1(\omega)^2 + \varepsilon_2(\omega)^2} - \varepsilon_1(\omega)\right]^{1/2}$$

There is no absorption of photons at both axes till 2.0 eV, inside the outlawed energy band. One can observe highest and wide absorption bands in the spectra of absorption coefficient above 10.0 eV due to electronic transitions to conduction band from valance band. Very small absorption of photons is observed in lower ultraviolet region i.e. between 3.0 to 8.0 eV and strong absorption is present in high energy UV region i.e. above 10.0 eV.

Furthermore, difference of incident power and reflected power known as reflectivity $R(\omega)$ is also calculated for surface study of $Sn_{1-x}In_xSe$. The value of reflectivity $R(\omega)$ at zero frequency limit known as static reflectivity $R(0)$ can also be calculated from the spectra of reflectivity. Calculated values of static reflectivity $R^{xx}(0)$ and $R^{zz}(0)$ are approximately 0.256 and 0.4, respectively. Behavior of real part $\varepsilon_1(\omega)$ of complex dielectric function and reflectivity is similar to each other. Therefore, absorption coefficient $I(\omega)$ and reflectivity $R(\omega)$ are inversely proportional to each other which means that reflectivity have higher values in the region where absorption coefficient have lower values. Moreover, various small peaks are also present in the spectra of reflectivity $R(\omega)$ due to anisotropy of the material. However, reflectivity is maximum where $\varepsilon_1(\omega)$ is minimum due to the reason that band gap becomes zero and all the incident photons are reflected by the material in the metallic region.

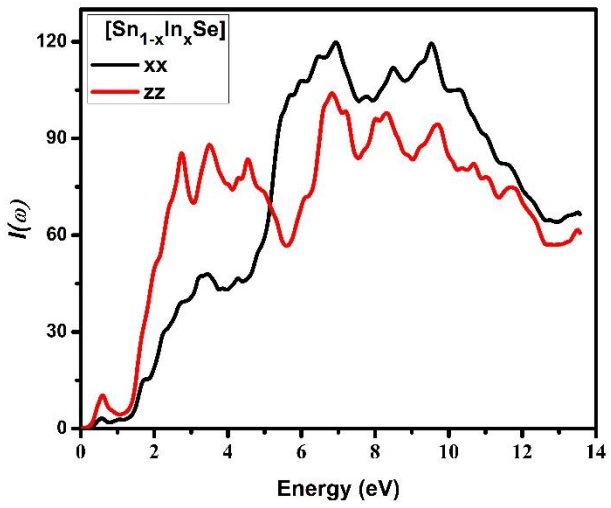

(a)

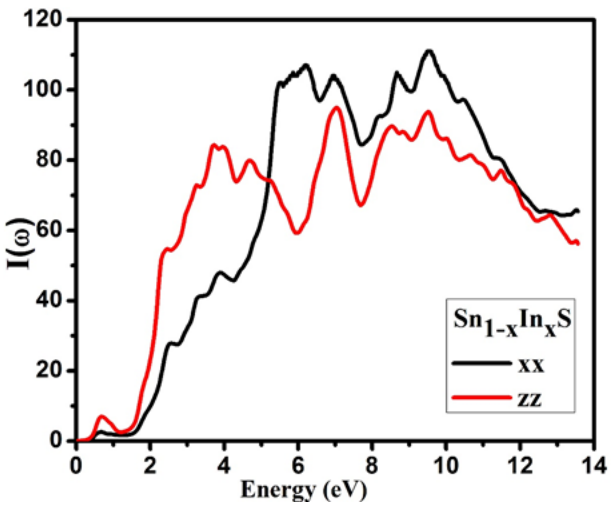

(b)

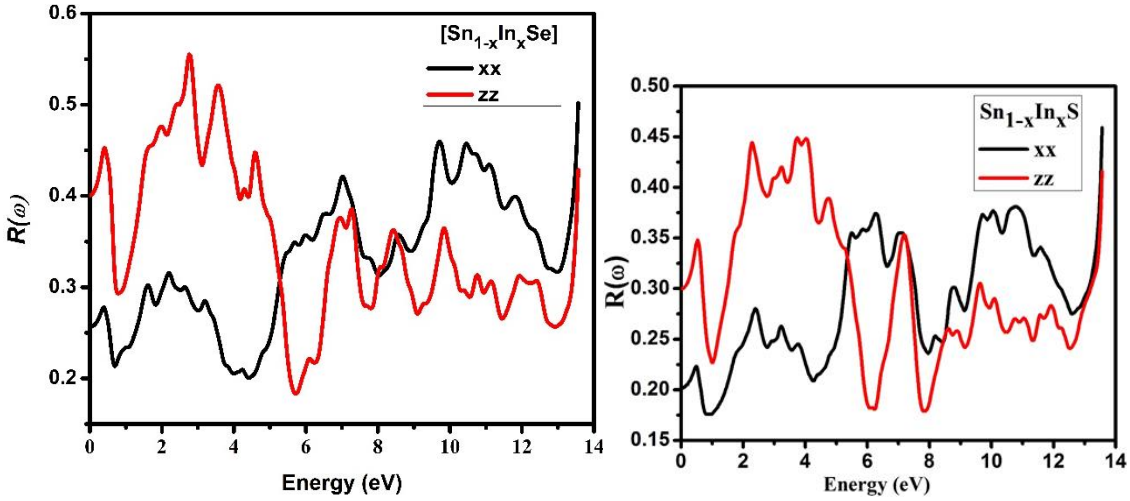

Fig. 7: (a) Absorption coefficient $I(\omega)$ and (b) reflectivity $R(\omega)$ for $Sn_{1-x}In_xSe$

The energy loss function $L(\omega)$ and optical conductivity $\sigma(\omega)$ are shown in Fig. 8 (a) and (b), respectively. Energy loss function $L(\omega)$ is considered as an important optical parameter that specifies the loss of energy by the fast moving electrons across the material. The peaks in the spectra of $L(\omega)$ contain characteristic behaviors that are associated with the plasma oscillations and the corresponding frequencies are known as plasma frequencies. Major peaks in the spectra of energy loss function $L(\omega)$ appears because of plasmon excitations. It is due to the mutual oscillations of the background atomic cores against the valance electrons in the longitudinal fashion with plasma frequency ω_p. One can notice from the spectra that there is no significant loss of energy by electrons up to 9.0 eV and then values of energy loss function $L(\omega)$ becomes maximum from 10.0 to 14.0 eV.

The optical conductivity $\sigma(\omega)$ is the measure of charge carriers produced as a result of breaking of bonds between the atoms of the material due to incoming photons that gives moderate forward current. We can see form Fig. 8 (b) that variations in the calculated spectra of optical conductivity $\sigma(\omega)$ shows similar behavior as that of imaginary part $\varepsilon_2(\omega)$, extinction coefficient $k(\omega)$ and absorption coefficient $\alpha(\omega)$, which illustrate that peaks in the spectra of optical conductivity $\sigma(\omega)$ arise due to absorption of incoming photons. Highest peaks in the spectra of optical conductivity $\sigma^{xx}(\omega)$ and $\sigma^{zz}(\omega)$ are present in near UV region and visible region.

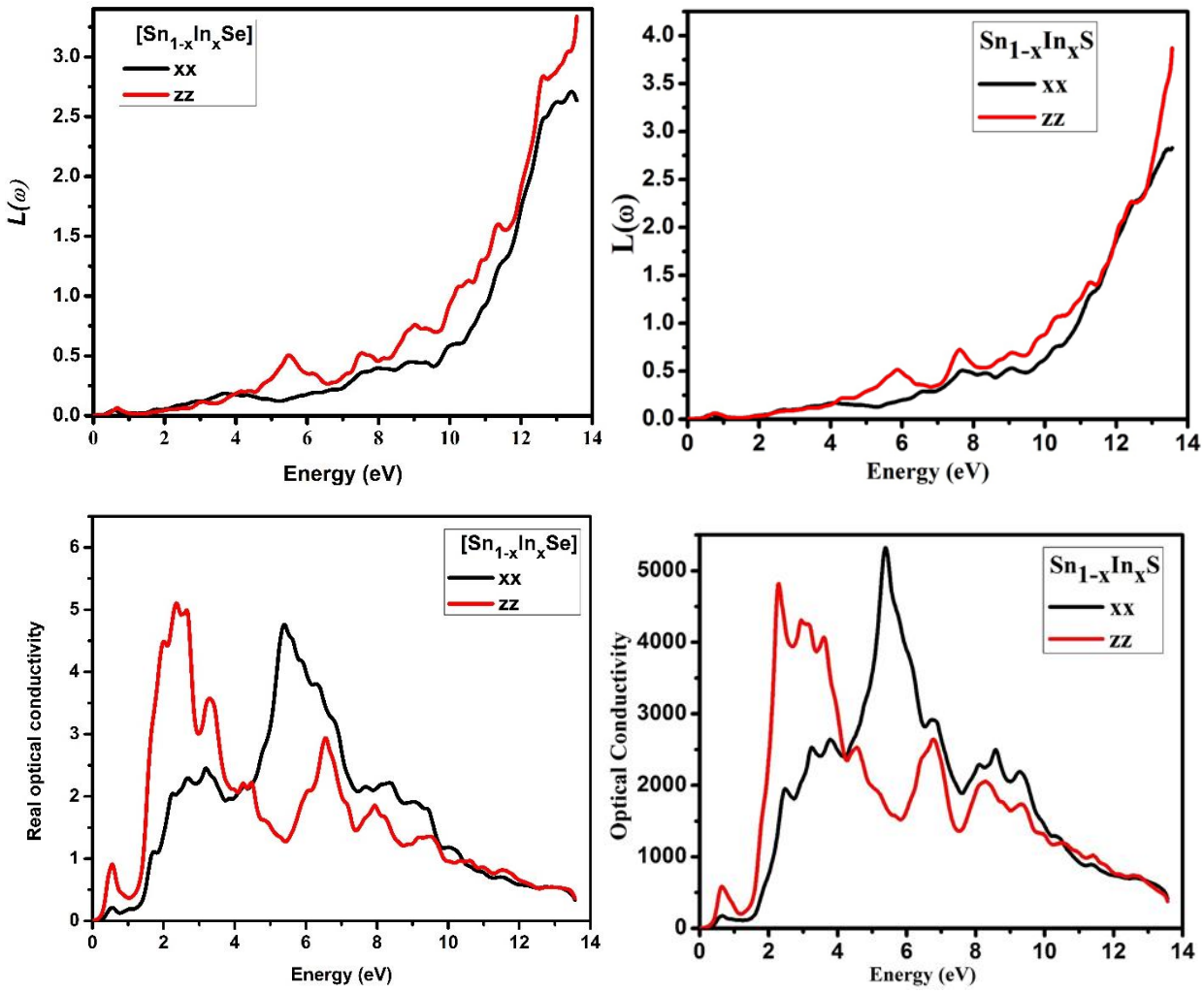

(a) (b)

Fig. 8: (a) Energy loss function $L(\omega)$ and (b) optical conductivity $\sigma(\omega)$ for $Sn_{1-x}In_xSe$

Conclusion

The exploration of the effects of the transition metals on structural and optical function dispersion of In doped SnS and SnSe materials have been performed using DFT based FP-LAPW approach within the GGA potential schemes. The electronic properties have shown the metallic nature. For the accurate calculations of the electronic structures i.e., band structures and density (Total and Partial) of states have been performed by employing the GGA functional. As we are interested in the optical properties of these materials, here we have discussed the results of spectral maxima positions.

The optical responses of are studied in terms of dielectric function dispersions ($\varepsilon(\omega) = \varepsilon_1(\omega) + \varepsilon_2(\omega)$) and other related optical properties ($I(\omega)$,

$L(\omega), R(\omega), n(\omega), K(\omega) and\ \sigma(\omega)$). The main peaks in the $\varepsilon_2(\omega)$, are due to electronic transitions from Sn/Se/S and In atoms.

REFERENCES

1. A. Luque, A. Marti, Phys. Rev. Lett. 78 (1997) 5014.
2. W. Shockley, H.J. Queisser, J. Appl. Phys. 32 (1961) 510.
3. A. Martı´, L. Cuadra, A. Luque, Proceedings of the 28th IEEE Photovoltaics Specialists Conference, vol. 940, IEEE, New York, 2000;
4. K. M. Yu, W. Walukiewicz, J. Wu, W. Shan, J. W. Beeman, M. A. Scarpulla, O. D. Dubon, P. Becla, Phys. Rev. Lett. 91 (24) (2003) 246403-1.
5. O. K. Andersen, Phys. Rev. B 42(1975) 3063-3083.
6. P. Hohenberg, W. Kohn, Phys. Rev. B 136 (1964) 864-871.
7. W. Kohn, L. J. Sham, Phys. Rev. 140 (1965) A1133-A1138.
8. P. Blaha, K. Schwarz, P. Sorantin, S. K. Trickey, Comput. Phys. Commun. 59 (1990) 339-415.
9. P. Blaha, K. Schwarz, G. H. Madsen, D. Kvasnicka, J. Luitz, in: WIEN2k, an Augmented Plane Wave Plus Local Orbitals Program for Calculating Crystal Properties, Vienna University of Technology Vienna, Austria (2001).
10. A.C.M. Padilha, H. Raebiger, A.R. Rocha, G.M. Dalpian, Charge storage in oxygen deficient phases of TiO2: defect Physics without defects, Sci. Rep. 6 (2016) 28871.
11. E.G. Ladopoulos, D. Str, Stationary energy storage by next generation lithium – ion batteries with intermediate bands, Univ. J. Computat. Anal. 5 (2017) 12–19.
12. F. K. Butt, A. S. Bandarenka, J. Solid. Stat. Electro chem, DOI 10.1007/s10008-016- 3315-3.
13. Q. Mahmood, M. Yaseen, M. Hassan Asif Mahmood, Chin. Phys. B 26 (8) (2017) 087803.
14. E. Schreiber, O.L. Anderson, N. Soga, Elastic Constants and Their Measurements, first ed., McGraw-Hill, New York, 1973.
15. F. Wooten, Optical Properties of Solids, Academic Press, New York, 1972.
16. D.R. Penn, Phys. Rev. 128 (1962) 2093.

17. K. Xiong, J. Robertson, S.J. Clark, Appl. Phys. Lett. 89 (2006) 022907.
18. Sonali Saha, T. P. Sinha, And Abhijit Mookerjee / Phys. Rev. B, 62 (2000) 8828.